Experimental study of double-diffusive instability in sidewall heating

By CHARLES G. JEEVARAJ AND JÖRG IMBERGER

Centre for Water Research, University of Western Australia, Nedlands, WA 6009, Australia

The response of a salinity-stratified fluid to sidewall heating is examined. Experiments were conducted using a linear salt gradient alone and with a combination of salt and thermal gradient in which the thermal stratification destabilized the density. The dominant feature of the flow was intrusions which propagated into the interior of the fluid. These were studied using shadowgraph, vertical temperature and salinity profiles, and dye streaks. Using the theory for convection in a long shallow cavity, an expression is derived for the velocity of propagation of the intrusions. The mechanism by which intrusions merge is also discussed to explain the observed formation of wavy interfaces during merging.

1. Introduction

An experimental investigation of the instability induced by sidewall heating in a salt- and heat-stratified fluid was conducted. The study was motivated by a project aimed at optimizing the performance of a salt-gradient solar pond (referred to hereafter as a 'solar pond') (Schladow 1985; Schladow & Imberger 1987; Schladow 1988; and Sherman & Imberger 1990). Schladow (1985) reported temperature differences of 1 to 3 °C between the wall of the pond and the water at the same depth. It was thought that the instabilities produced by this sidewall heating were responsible for the observed sidewall intrusions, which in turn were thought to increase the transport of heat and salt from the bottom to the surface of the solar pond, decreasing the efficiency of the pond as a solar collector (see Turner 1985 for a review of double-diffusive processes).

Earlier laboratory studies of sidewall heating have been carried out by Thorpe, Hutt & Soulsby (1969), Chen, Briggs & Wirtz (1971), Huppert & Turner (1980), Paliwal & Chen (1980) and Tanny & Tsinober (1988) in a salt-stratified system (referred to hereafter as 'singly' stratified) with a constant-wall-temperature overheat. Similar experiments were also reported by Narusawa & Suzukawa (1981) and Suzukawa & Narusawa (1982) but with a constant heat flux at the sidewall. Thorpe *et al.* (1969) and Paliwal & Chen (1980) conducted their experiments in narrow slots, whereas all the others used wide tanks. In narrow slots, the large aspect ratio dominated the results and only the wide-tank experiments are relevant to the observed solar-pond instabilities. To understand clearly the instabilities in a solar pond, it was necessary to perform experiments in a fluid stratified with opposing gradients of temperature and salinity (referred to hereafter as 'doubly' stratified). In such cases it is possible that the unstable thermal stratification may supply potential energy to the intrusions when the sidewall heating is removed.

Chen *et al.* (1971) showed that in a singly stratified fluid the instability would commence when the magnitude of the Rayleigh number became larger than a critical
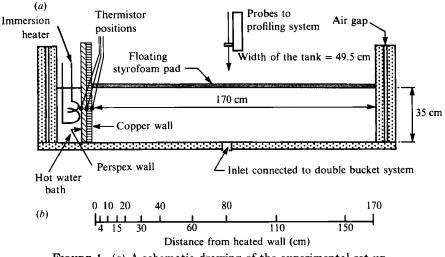
FIGURE 1. (a) A schematic drawing of the experimental set-up.
(b) Positions of profiling stations.

value. The Rayleigh number was defined using a lengthscale based on the height of rise attained by a parcel of fluid, heated by the sidewall, in the given ambient density gradient. These authors showed that the initial thickness of the intrusions scaled with this length. The constant of proportionality between the actual layer thickness and this lengthscale was found to lie between 0.75 and 0.98 for a Rayleigh-number range of 1.4×10^4 to 5.4×10^4. Huppert & Turner (1980) and Huppert, Kerr & Hallworth (1984) performed similar experiments but at much higher Rayleigh numbers ($> 10^6$) using fluids with different physical properties, and showed that the factor of proportionality fluctuated between 0.5 and 0.7.

Wirtz & Reddy (1979) observed that the initiated intrusions were unstable and quickly merged to form much bigger, stable layers which had well-mixed interiors and sharp interfacial gradients, with a flow in the interior similar to that observed in a low-aspect ratio enclosure (Imberger 1974); the fluid rose along the hot wall, travelled along the top boundary of the intrusion, descended as it lost heat to its neighbour and then returned along the bottom boundary to the heated wall. The convective circulation inside the layers was observed to be much faster than the propagation velocity of the intrusions. Linden & Weber (1977) presented measurements of the intrusion velocity for the case where the intrusion was triggered by a sloping wall. They found that the velocity was constant for a particular experimental configuration, but increased with decreasing initial strength of the density gradient. Suzukawa & Narusawa (1982) also found that the propagation velocity of the layer front was constant with time, but in their case it was seen to increase with the magnitude of the applied heat flux at the sidewall. These observations were explained with a model for the velocity of propagation obtained by balancing the horizontal heat flux through the sidewall with the rate of heat capture at the front, assuming that the intrusion layer was of constant thickness.

Merging of the unstable adjacent layers to form a stable layered system has been previously observed by Wirtz & Reddy (1979) in narrow-slot experiments. Turner & Chen (1974) also qualitatively described merging of layers in a sugar–salt system. The recent study of Tanny & Tsinober (1988) categorized merging as 'first' and 'subsequent' merging and proposed a Rayleigh-number criterion for the first

merging to occur. In contrast to the observations of Wirtz & Reddy (1979), they concluded that the subsequent merging did not lead to a doubling of layer thickness.

In a doubly stratified case with opposing density gradients due to salinity and temperature, an instability triggered by the sidewall heating (external source) could be powered and sustained in motion by the initial vertical temperature gradient (internal source). Hence, it was hypothesized that in the doubly stratified case sidewall heating is only necessary to create an instability. Later, even if the heat flow through the sidewall were shut down, the layer would continue to propagate, deriving its energy from the initial thermal stratification (Turner & Chen 1974). This hypothesis was also tested in the present study.

Thus, the aims of the present study were: (a) to establish experimentally in a wide tank (for both singly and doubly stratified cases) the criteria for the formation of intrusions and to observe the merging patterns and the structure of the initial and developed layers as well as the interfaces; (b) to determine an expression for the velocity of propagation of the intruding layers; (c) to observe the behaviour of the layers in a doubly stratified system once the heat flow through the sidewall was removed.

2. Description of the experiments

The experimental apparatus is shown schematically in figure 1 (a). The inner glass (10 mm thick) was separated from the outer glass by a 5 mm air gap. The tank was partitioned with a 2 mm thick copper and 9.6 mm thick Perspex sandwich wall, which was used to form a constant-temperature bath at one end of the tank. To measure the heat flux across this partition, five thermistors were placed at different positions: one inside the constant-temperature bath, three between the copper and Perspex walls, and one attached to the copper wall facing the ambient fluid. The side serving as the constant-temperature bath was stirred continuously and heated with an immersion heater. The endwalls, the bottom and the surface of the tank were all insulated with Styrofoam.

In a typical experiment the tank was filled from the bottom using the standard two-tank method to achieve the desired temperature and salinity gradients. For the singly stratified case, one tank contained fresh and the other salty water, both of the same temperature, whereas for the doubly stratified case, one tank contained cool fresh water and the other hot salty water. Conductivity and temperature profiles were obtained with a four-electrode-type conductivity probe (Head 1983) and a fast-response thermistor (Thermometrics FP07). The thermistor and the conductivity probes were connected to a 12 bit A-D board via a pre-amplifier. This yielded a resolution of 0.005 °C and 0.001 S m^{-1} respectively (Carter & Imberger 1986). These sensors were mounted on a carriage which could be moved with a programmable stepper motor. In general the sensors were moved through the water column with a speed of 20 mm s^{-1} and data were collected at 20 Hz, yielding a vertical resolution of 1 mm. Profiles were collected along the centreline of the tank at the horizontal positions, shown in figure 1 (b). The conductivity and temperature signals were used to calculate salinity using the algorithm developed by Millero & Poisson (1981).

A shadowgraph technique was used to determine the onset of intrusion layers and also to measure their initial thicknesses; the size of the layers at onset was obtained by counting the number of layers within a known distance. In the later stages of the experiments, the size of the layers was obtained from the temperature and the salinity profile data; the thickness was defined as the distance between two adjacent
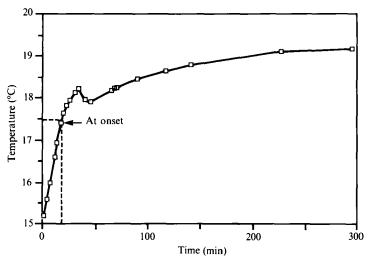
FIGURE 2. The response of the thermistor attached to the side of the copper wall facing the ambient fluid for experiment 236.

strong gradient surfaces. Locating the position of the layer front from the shadowgraph was found to be extremely difficult and therefore the layer front was inferred from the vertical temperature profiles. When the intruding layers had extended more than 30 cm into the fluid, small crystals of potassium permanganate dye were dropped into the tank, and a sequence of photographs was taken which allowed the determination of the velocity profile inside and in front of the layers.

To study the effect of removal of the sidewall heating, the copper wall was separated from the constant-temperature bath by inserting a Styrofoam pad between the Perspex wall and the bath and then rapidly draining the water from the bath.

3. Results

3.1. *General observations*

As a preliminary to an experiment the constant-temperature bath was brought to the desired temperature with the Styrofoam pad in place. To initiate the experiment the insulating pad was quickly removed; the temperature of the copper surface facing the experimental fluid then rose gradually as shown in figure 2. Potassium permanganate crystals introduced adjacent to the copper wall sharpened the shadowgraph picture and made it possible to identify the instant of initiation of the intrusions. As the temperature of the copper wall was raised beyond the threshold value rapid merging of layers always continued to take place until stable intrusions moved horizontally into the tank. The cessation of this initial merging corresponded to the observed 'dip' in the temperature time series shown in figure 2. Initially the heat was conducted away from the wall, but immediately after the appearance of layers and during the merging period, the rate of heat transfer progressively increased as the layers started to grow outwards, sharpening the conductive layer near the copper wall, and removing the heat by convection (Patterson & Imberger 1980). The increased heat transfer caused a slight lowering of the wall temperature, which then rose again as the intrusion moved into the tank, increasing the heat transfer path.
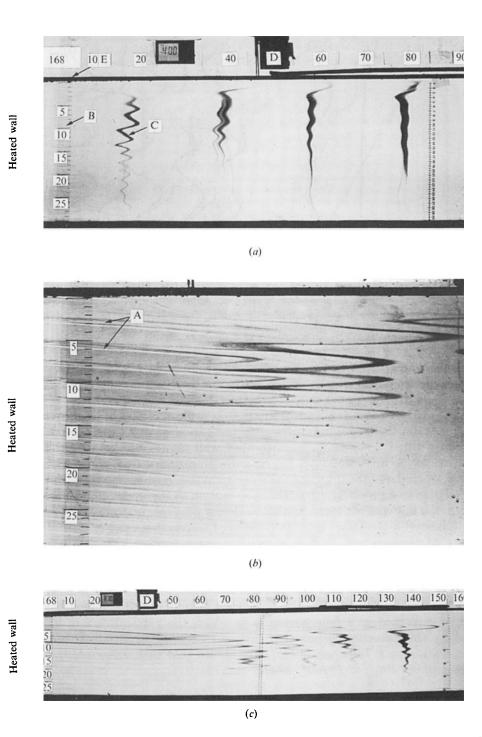
(a)

(b)

(c)

FIGURE 3. The onset of layers and their development in experiment 168 with a salinity gradient heated from the side. (a) $t' = 13$ min. (b) a close up, $t' = 93$ min. (c) $t' = 283$ min. (A, layer interface; B, approximate position of layer front; C, columnar waves (shear) felt far ahead of the layer front; D, vertical profiling system with probes; E, insulation pad.)
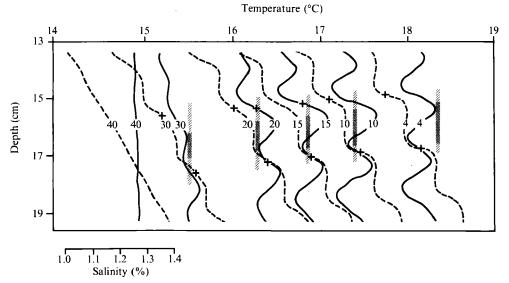
FIGURE 4. Raw vertical temperature (solid line) and salinity (dotted line) data inside a layer when a salinity gradient is heated from side (experiment 236). Approximate layer interface is denoted by +, ▧ is the well-mixed region and ▨ denotes the sharp density gradient region. Numbers on the curves indicate the horizontal positions of the profiling stations.

In the singly stratified experiments, the layers appeared simultaneously after a few minutes, over the entire depth of the wall. The results from one experiment are shown sequentially in figure 3. As described above, when the temperature rose beyond the critical value for layer formation, a rapid merging of layers was noted, but the intrusion thickness stabilized after the period of rapid merging. The layers were slightly tilted downwards from the hot wall (figure 3b) because the average temperature of the intruding layer decreased with distance from the wall. The layer shape was tapered and the propagation velocity of the front decreased with time. The dye line visible in figure 3(b) shows that the motion in the upper part of a layer was away from the hot wall while the fluid in the lower part moved towards the wall. This clearly indicated a clockwise cellular pattern of convection.

The set of temperature profiles shown in figure 4 reveals the decrease in the difference between maximum and minimum temperatures along the length of an intrusion. As the vertical temperature difference is small compared to the horizontal variation between the hot wall and the ambient fluid, it is evident that the warmer fluid flowing in the upper part of the layer loses heat to the return flow in the lower part. This characterizes a flow structure in which the vertical flux of vorticity is balanced by the baroclinic generation supported by the longitudinal temperature gradient. Patterson & Imberger (1980) have shown that such a flow occurs when the Rayleigh number $Ra_{H_0} < (Pr/A)^4$, where

$$Ra_{H_0} = \frac{g\alpha(T_w - T_\infty)H_0^3}{\nu\kappa_T},$$ (1)

in which H_0 is the layer thickness, A is the aspect ratio of the layer, Pr is the Prandtl number, T_w and T_∞ are the temperatures of the wall and the unaffected ambient fluid respectively, g is the acceleration due to gravity, α is the coefficient of thermal
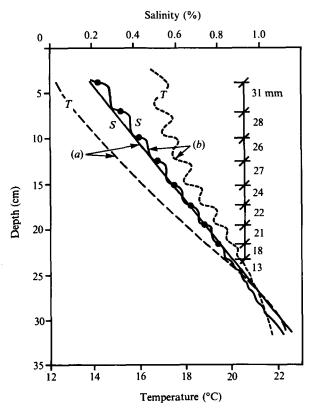
FIGURE 5. Raw temperature (*T*) and salinity (*S*) data for doubly stratified experiment 218. The decreasing layer thickness with depth is shown here: ●, the approximate interface position. (*a*) Initial condition; (*b*) Condition after 3 h.

expansion, ν is the kinematic viscosity, and κ_T is the thermal diffusivity. The salinity profiles in figure 4 indicate that the interior of the intrusions was well mixed, but sharp-gradient regions separated individual intrusions. However, the tapered shape of the layers meant that the thickness of the sharp-gradient region increased with distance from the wall.

The waviness of the dye lines far ahead of the layer front (figure 3*c*) was due to a shear flow ahead of the intrusion with a wavelength of the order of the thickness of layers. Akbarzadeh & Mannins (1988) and Tanny & Tsinober (1988) observed similar shear flows. These were induced by propagating columnar shear waves which moved out ahead of the intrusions. The average horizontal shear velocity associated with the shear waves, 4 cm from the heated wall, just after the onset of layers and immediately in front of the intrusion, was observed to be about one-third of the speed of the front of the intrusion layers. The density profiles derived from the salinity and temperature profiles ahead of the intrusion fronts indicated that the propagating columnar waves did not induce any measurable change in the density field.

In the doubly stratified experiments (cold/fresh on top of hot/salty) the difference in temperature across the wall between the constant-temperature bath and the working fluid varied with depth. Therefore the layer formation began at the top and then proceeded downward with time. Figure 5 shows the temperature and salinity profiles taken before (figure 5*a*) and after (figure 5*b*) the sidewall heating was turned

FIGURE 6. Formation of double-diffusive layers due to sidewall heating at
$t' = 46$ min in doubly stratified experiment 218.

on in a doubly stratified experiment. As the temperature difference due to sidewall heating was higher at the top, the stable layers that started growing outwards showed higher velocities and thicknesses at the top than at the bottom (figure 6). Apart from these differences, the behaviour was similar to the singly stratified cases.

When the heat flow through the sidewall was removed, the propagation of the intrusion layers quickly stopped and the sharp interfaces marking the boundaries of the intrusions faded; the fading being most rapid near the copper wall. This was observed in both singly and doubly stratified systems, from both the shadowgraph photographs and from the profile data. This shows, contrary to our expectation, that the energy available from the unstable thermal stratification of the doubly stratified system was inadequate to sustain the convective motion initially triggered by the sidewall heating.

Exp. no.	T_∞ (°C)	T_w (°C)	$\phi_0 \times 10^2$ (m^{-1})	H_0 (mm)	η (mm)	$C = H_0/\eta$	$Ra_\eta \times 10^{-4}$
33	27.9	29.25	5.0	7.0	8.1	0.87	2.34
168	19.9	21.6	4.4	8.0	9.1	0.88	2.05
169	19.8	21.5	4.9	8.0	8.32	0.96	1.63
236	14.9	17.5	4.5	8.5	9.7	0.88	2.36
259	16.4	18.3	4.1	7.5	8.34	0.89	1.22
260	16.4	17.9	2.9	8.8	9.31	0.94	1.26
210	16.2	17.3	1.8	10.0	12.84	0.78	3.03
218	15.5	16.6	1.8	11.0	13.7	0.8	3.81
229	16.8	17.8	1.4	12.0	15.26	0.78	4.7

TABLE 1. The experimental parameters and results at the onset of instability. First and second groups are from singly and doubly stratified experiments respectively.

Exp. no.	Time (min)	T_∞ (°C)	T_w (°C)	H_0 (mm)	η (mm)	$C = H_0/\eta$	$Ra_{H_0} \times 10^{-4}$	A	$Pr^4 A^{-4}$
168	309	19.9	24.5	21.0	28.2	0.74	7.7	0.047	4920
169	42	19.8	23.8	18.0	20.04	0.81	3.7	0.13	84
236	499	14.9	20.2	19.0	25.9	0.73	4.7	0.03	29642
259	71	16.4	19.9	14.0	16.13	0.87	1.1	0.17	29
210 (L6)	45	16.2	18.5	18.0	22.5	0.8	1.97	0.18	23
218 (L4)	285	15.5	20.3	29.0	45.6	0.64	15.5	0.05	3842
229 (L5)	485	16.8	18.9	24.0	36.9	0.65	4.0	0.06	1850

TABLE 2. A typical set of the experimental data and results after intrusions had been established. First and second groups are from singly and doubly stratified experiments respectively. Each layer is treated individually in a doubly stratified experiment and the relevant layer is identified in parentheses.

3.2. *Onset of instability and the layer thickness*

Chen *et al.* (1971) defined the lengthscale for layer thickness as

$$\eta = \frac{\alpha(T_w - T_\infty)}{\phi_0}, \tag{2}$$

where $\phi_0 (= -(1/\rho_0)(\partial\rho/\partial z'))$ is the ambient density gradient, ρ_0 is the mean density, ρ is the fluid density, and z' is the vertical coordinate. The quantity η represents the height of rise of a parcel of fluid with a temperature anomaly equal to $(T_w - T_\infty)$. The Rayleigh number, defined by

$$Ra_\eta = \frac{g\alpha(T_w - T_\infty)\eta^3}{\nu\kappa_T}, \tag{3}$$

was computed at the onset of the layer formation for singly and doubly stratified experiments before merging took place and is given in table 1. Chen *et al.* (1971) proposed a critical value of $1.5 \pm 0.25 \times 10^4$, which is slightly lower than that observed in the present experiments which exhibited a mean value of $Ra_\eta = 1.8 \pm 0.5 \times 10^4$, for a singly stratified system. For a doubly stratified case, higher onset Rayleigh numbers and somewhat lower values of the ratio $C = H_0/\eta$ were obtained. In every experiment, the wall temperature was raised beyond the
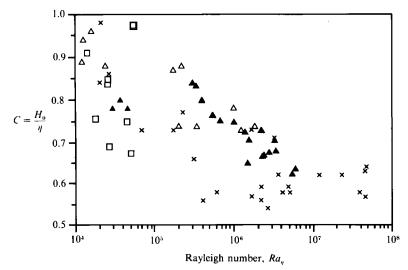
FIGURE 7. The dependence of C on Rayleigh number Ra_η: $\triangle$, singly stratified experiments; $\blacktriangle$, doubly stratified experiments; $\times$, Huppert & Turner (1980); $\square$, Chen et al. (1971).

threshold value for layer formation in order to increase the velocity of propagation of the intruding layers. Over a 10 h experiment, this allowed the layers to cover a reasonable proportion of the length of the tank. This relatively bigger value of $(T_w - T_\infty)$, caused the layer thickness to increase owing to merging. Table 2 lists the parameters after the intrusions had become well established.

The value of C is plotted against Ra_η in figure 7 along with the data points from other investigators. The data include values of C for layers both at onset and at the well-developed stage for both singly and doubly stratified systems. In general, figure 7 suggests a tendency for C to decrease as Ra_η increases. For the doubly stratified case, the heat flow through the sidewall decreased the mean vertical temperature gradient (see figure 5), thus increasing the mean vertical density gradient. The value of η computed from (2) using the initial value of density gradient would thus be an overestimate leading to a smaller value of C. However, this effect was small compared to the scatter between data from different investigators.

As discussed earlier, once a stable layer had formed, the top and bottom interfaces became very sharp, acting as boundaries to the convective motion within the intrusion. For example, in a typical experiment the initial value of the density stability ratio

$$R_\rho = \frac{\beta \Delta s}{\alpha \Delta T}, \qquad (4)$$

was about 3.3. Here β is the salinity contraction coefficient $(1/\rho)(\partial\rho/\partial s)$ and Δs and ΔT are the salinity and temperature differences respectively between two vertical points. This ratio increased to 4.4 across the gradient zones after the intrusions had become well established.

3.3. Propagation speed of intrusion

The salinity profile data were used to determine the position of the layer interfaces, defined here as the midpoint of the sharp salt-gradient region. The temperature inside each layer was then averaged vertically. Typical longitudinal variations of the
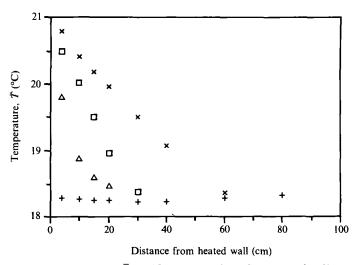
FIGURE 8. Average temperature ($\bar{T}$) inside a layer plotted against the distance from the heated wall for the singly stratified experiment 168: $+$, initial; $\triangle$, $t' = 17$ min; $\square$, $t' = 96$ min; $\times$, $t' = 210$ min.
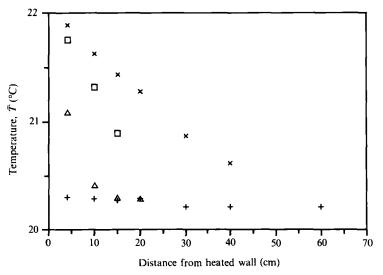

FIGURE 9. Average temperature ($\bar{T}$) inside a layer plotted against the distance from the heated wall for doubly stratified experiment 210: $+$, initial; $\triangle$, $t' = 70$ min; $\square$, $t' = 120$ min; $\times$, $t' = 310$ min.

depth-averaged temperature are shown in figures 8 and 9 for singly and doubly stratified cores. The data show that away from the wall, in the main part of the intrusion, the average temperature varied linearly with distance from the wall. It can also be seen in figure 8 that the average temperature gradient decreased with time as the layer intrusion advanced into the tank. The presence of a linear temperature gradient and the nature of the convective gyre observed from the dye streaks suggested that the motion could be likened to convection in a long box heated and cooled at opposite sides (Imberger 1974). However, in our case the length of the box, the intrusion length, increased slowly with time, modulating the convection pattern inside the intrusion.

Patterson & Imberger (1980) discussed various possible flow regimes depending on the aspect ratio A of the enclosure and the values of the Rayleigh numbers. Table 2 lists the values of these parameters for the intrusions studied; the criterion $Ra_{H_0} < (Pr/A)^4$ is clearly satisfied in all cases.

Assuming that the rate of propagation of the intrusion is much slower than the timescale of the convective circulation inside a layer, and the taper of the intrusions is small enough to be neglected to first order, we may introduce the following non-dimensional quantities:

$$x = \frac{x'}{L'}, \quad z = \frac{z'}{h}, \quad \theta = \frac{T - T_\infty}{T_w - T_\infty},$$

$$u = \frac{u'L'}{\nu Gr}, \quad w = \frac{w'L'}{\nu Gr},$$

where L' is the length of the intrusion, h is the local thickness at station x' and Gr is the local Grashof number defined below. With these scales, the governing equations for the stream function, ψ, and the vorticity, ω, at steady state are

$$Gr\, A^2 \frac{\partial(\omega, \psi)}{\partial(x, z)} = A^2 \frac{\partial^2 \omega}{\partial x^2} + \frac{\partial^2 \omega}{\partial z^2} + \frac{\partial \theta}{\partial x}, \tag{5}$$

$$A^2 \frac{\partial^2 \psi}{\partial x^2} + \frac{\partial^2 \psi}{\partial z^2} = -\omega, \tag{6}$$

$$Pr\, Gr\, A^2 \frac{\partial(\theta, \psi)}{\partial(x, z)} = A^2 \frac{\partial^2 \theta}{\partial x^2} + \frac{\partial^2 \theta}{\partial z^2}, \tag{7}$$

where
$$Gr = \frac{g\alpha(T_w - T_\infty)\, h^3}{\nu^2}, \quad Pr = \frac{\nu}{\kappa_T}, \quad A = \frac{h}{L'},$$

and
$$\omega = A \frac{\partial w}{\partial x} - \frac{\partial u}{\partial z}, \quad u = \frac{\partial \psi}{\partial z}, \quad w = -A \frac{\partial \psi}{\partial x}. \tag{8}$$

The above equations are subject to the following boundary conditions:

$$\theta = 1, \quad x = 0; \quad \theta = 0, \quad x = 1 \tag{9}$$

$$\psi = \frac{\partial \psi}{\partial z} = \frac{\partial \psi}{\partial x} = 0, \quad \theta = 1 - x; \quad z = 0, 1. \tag{10}$$

The motivation for (10) is the assumption that the vertical heat flux through the bottom is lost entirely through the top boundary and that the temperature at these boundaries assumes a value equal to the average value at that section. Comparison of the top and bottom temperature gradients of adjacent layers showed only a 10% error in this assumption. Considering the dimension of the wide tank, this error is within reasonable limits. Following Cormack, Leal & Imberger (1974), we assume that all variables can be expressed by a regular expansion in the small parameter A:

$$\theta = \theta_0 + A\theta_1 + A^2\theta_2 + \dots, \tag{11}$$

$$\psi = \psi_0 + A\psi_1 + A^2\psi_2 + \dots, \tag{12}$$

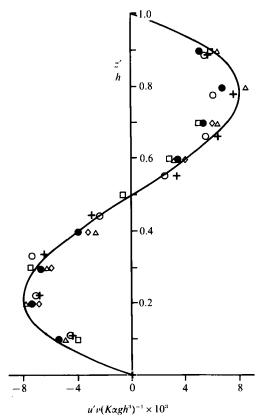$$\omega = \omega_0 + A\omega_1 + A^2\omega_2 + \dots. \tag{13}$$

Figure 10. Non-dimensional plot of velocity inside a layer *vs.* the vertical distance above the bottom interface of that layer. ———, Theoretical prediction (equation (14)). Data from singly stratified experiment 236; $+$, $d = 13.3$ cm ($x = 0.29$); $\bigcirc$, $d = 9.8$ cm ($x = 0.22$); $\bullet$, $d = 13.3$ cm ($x = 0.57$); $\square$, $d = 9.8$ cm ($x = 0.44$). Data from doubly stratified experiment 229: $\triangle$, $d = 8.2$ cm ($x = 0.27$); $\diamond$, $d = 8.2$ cm ($x = 0.54$). (Here d is the depth of the layer from the water surface and $x = x'/L'$.)

Substituting (11), (12) and (13) into (5), (6) and (7) and applying the boundary conditions, we obtain the following expressions for velocity to first order:

$$u' = -\frac{g\alpha K h^3}{\nu}(\tfrac{1}{6}z^3 - \tfrac{1}{4}z^2 + \tfrac{1}{12}z), \tag{14}$$

and the temperature to second order:

$$T = T_\infty + (T_w - T_\infty)(1-x) + \frac{K^2 g\alpha h^5}{\nu\kappa_T}(\tfrac{1}{120}z^5 - \tfrac{1}{48}z^4 + \tfrac{1}{72}z^3 - \tfrac{1}{720}z), \tag{15}$$

where $K = -\mathrm{d}\bar{T}/\mathrm{d}x'$, is a function of t'; $\bar{T}$ is the temperature averaged vertically within a layer. All the velocity and temperature data inside a layer are plotted non-dimensionally in figures 10 and 11 respectively. For the theoretical comparison, in (15) the vertically averaged value of the measured temperature (T_0) was used instead of $T_\infty + (T_w - T_\infty)(1-x)$. Data from both the singly and doubly stratified cases are included. The comparison between observations and predictions is generally excellent. Noteworthy is the similarity of (14) and (15) with (1) and (2) of Imberger
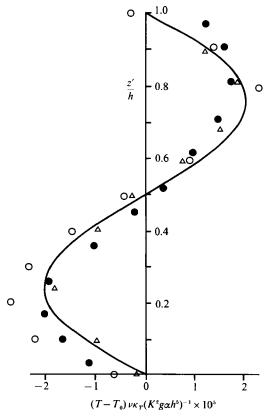
FIGURE 11. Non-dimensional plot of temperature inside a layer *vs.* the vertical distance above the bottom interface of that layer. ———, Theoretical prediction (equation (15)). Data from singly stratified experiment 236: $\bigcirc$, $d = 11.0$ cm ($x = 0.1$); $\triangle$, $d = 11.0$ cm ($x = 0.5$). Data from doubly stratified experiment 229: $\bullet$, $d = 13.3$ cm ($x = 0.47$). (Here d is the depth of the layer from the water surface and $x = x'/L'$.) T_0 is the measured, vertically averaged temperature.

(1974); only the shape of the temperature profile is different, a difference introduced by the application of the conducting upper and lower boundary condition.

We shall now use the above solution to construct a global solution which allows h to vary with x' and time. Given the values of the Rayleigh number and aspect ratio in table 2, convection was the dominant mode of longitudinal heat transfer within the intrusion. The horizontal flux across any section is thus given by:

$$F = c_p \rho_0 \int_0^h u'[T - T_\infty - (T_w - T_\infty)(1 - x')]\,\mathrm{d}z'. \tag{16}$$

Substitution from (14) and (15) yields

$$F = \frac{c_p \rho_0 g^2 \alpha^2 K^3 h^9 C_1}{\kappa_T \nu^2}, \tag{17}$$

where $\quad C_1 = -\int_0^1 \{(\tfrac{1}{120}z^5 - \tfrac{1}{48}z^4 + \tfrac{1}{72}z^3 - \tfrac{1}{720}z)(\tfrac{1}{6}z^3 - \tfrac{1}{4}z^2 + \tfrac{1}{12}z)\}\,\mathrm{d}z = -8.27 \times 10^{-7}. \tag{18}$

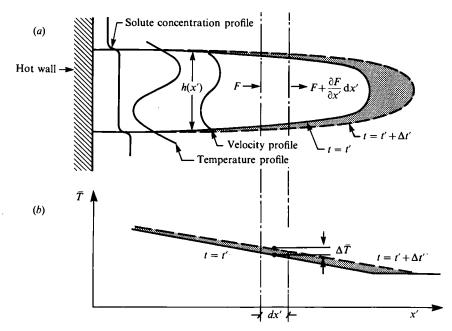The sketch of a single intrusion in figure 12 (*a*) illustrates how a layer advances into

FIGURE 12. (*a*) A sketch of a propagating layer. (*b*) A sketch of the average temperature inside the layer against horizontal distance from heated wall.

the tank (the shaded area); the outwardly flowing warmer fluid heats up the ambient fluid at the front of the intrusion. Figure 12(*b*) shows the resulting change in the average temperature gradient. Hence, the heat gain by an element length dx' can be written as

$$\frac{\partial F}{\partial x'} = -\rho_0 c_p \frac{\partial \bar{T}}{\partial t'} h(x').$$ (19)

Substituting from (17), differentiating with respect to x' and inserting the definition of $K = (-d\bar{T}/dx')$ yields

$$\frac{\partial}{\partial x'}\left[\frac{9g^2\alpha^2K^3C_1 h^7}{\nu^2\kappa_T}\frac{\partial h}{\partial x'}\right] = \frac{\partial K}{\partial t'}.$$ (20)

Integrating (20) twice with respect to x' assuming that K is independent of x' and using boundary conditions at $x' = 0$,

$$\frac{\partial h}{\partial x'} = 0,$$ (21)

$$h = H_0,$$ (22)

leads to the result
$$(x')^2 = \frac{9}{4}\frac{g^2\alpha^2K^3C_1}{\nu^2\kappa_T[\partial K/\partial t']}H_0^8\left[1 - \frac{h^8}{H_0^8}\right].$$ (23)

The above equation gives the shape of the layer. Assuming further that the end region at the front of the intrusion is small (Cormack *et al.* 1974) then the length of the intrusion is given from (23) by setting $h = 0$ at $x' = L'$, so that

$$(L')^2 = \frac{9}{4}\frac{g^2\alpha^2K^3C_1}{\nu^2\kappa_T[\partial K/\partial t']}H_0^8,$$ (24)
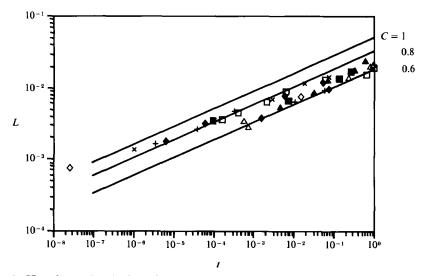
FIGURE 13. Non-dimensional plot of the position of the layer front vs. elapsed time from the instant of the onset of instability. ——, equation (28) for various C. For singly stratified experiments: ■, exp. no. 168; □, exp. no. 236; ▲, exp. no. 259; △, exp. no. 260. For doubly stratified experiments: ×, exp. no. 210 (layer 2); ◆, exp. no. 218 (layer 4); +, exp. no. 218 (layer 5); ◇, exp. no. 229 (layer 2).

where K can be expressed as $(T_w - T_\infty)/L'$ since Ra_{H_0} was small (Cormack *et al.* 1974). Now treating L' as a function of t', (24) may be written as

$$(L')^3 \frac{dL'}{dt'} = -\frac{9}{4} \frac{g^2 \alpha^2 (T_w - T_\infty)^2 C_1}{\nu^2 \kappa_T} H_0^8. \tag{25}$$

Integrating the above with respect to t' and using $L' = 0$ at $t' = 0$ yields

$$(L')^4 = -9 \frac{g^2 \alpha^2 (T_w - T_\infty)^2 C_1}{\nu^2 \kappa_T} H_0^8 t'. \tag{26}$$

Setting
$$H_0 = \frac{C\alpha(T_w - T_\infty)}{\phi_0}, \tag{27}$$

as suggested by Chen *et al.* (1971), and verified in §3.2, leads to the following non-dimensional intrusion-length expression:

$$L^4 = -9C^8 C_1 t, \tag{28}$$

where
$$L = L'\phi_0, \quad t = \frac{g^2 \alpha^{10}(T_w - T_\infty)^{10}}{\phi_0^4 \kappa_T \nu^2} t'.$$

The non-dimensional horizontal position of layer fronts plotted against the elapsed non-dimensional time is shown in figure 13 for both the singly and doubly stratified cases. The average length of the layers was taken as L' for singly stratified experiments, whereas an individual layer length was chosen for each doubly stratified case because each layer had a different length. For comparison (28) is drawn in figure 13 with values of the constant C equal to 1, 0.8 and 0.6: most of the experimental data lie within a value of $C = 0.8$ and 0.6.

The general behaviour of the data points agrees well with the $\frac{1}{4}$-power derived above. However, the departure at the initial stages of growth should be noted; the aspect ratio was insufficiently small to make the long-box analysis valid. In the Appendix we give a comparison of Suzukawa & Narusawa's (1982) experimental data for the propagation velocity of the intrusion layers with a similar analysis, but with the constant-flux boundary condition at $x = 0$; again there is good agreement.

3.4. *The merging of layers*

We have discussed the merging of intrusive layers as the wall temperature rose above the critical value towards steady state. This was classified as 'first' merging and it was observed to occur uniformly along the entire vertical sidewall.

After stable layers had become established, the temperature of the sidewall increased further and the additional buoyancy received by the fluid was greater than could be accommodated by the existing intrusions which were, however, constrained vertically by the top and bottom stable density interfaces. This led to an unstable situation which eventually relaxed through merging across the weakest interface, the interface with the smallest density gradient. In this 'subsequent' merging, the thickness of the layer formed was not simply the sum of the two merged layers, but rather the layers in the neighbourhood adjusted and eventually attained a new thickness in equilibrium with the increased wall temperature. A similar sequence of events was reported by Tanny & Tsinober (1988). From the temperature profiles taken during merging, the convective pattern and the heat transfer may be inferred. From the shadowgraphs it was seen that the merging process commenced with one layer propagating slightly faster than its neighbour immediately below, and subsequently merging together.

A typical experimental observation of this process is shown in figure 14 (*a–c*) which shows the temperature profiles taken vertically across layers at different instances, illustrating a merging of layers 1 and 2. The arrows in figure 14 (*a*) indicate the general direction of convective motion within layers prior to merging. Consider the temperature profiles at 4 cm (the horizontal distance from the heated wall) in figures 14 (*a*) and 14 (*b*). Two consecutive temperature maxima and minima across layers 1 and 2 in figure 14 (*a*) became one in figure 14 (*b*). However, the other temperature profiles taken at 10, 15 and 20 cm show temperature distributions that were less pronounced, which indicates a weaker convective motion. From these profiles a new convective pattern can be constructed, as illustrated by loops x and y in figure 14 (*b*); the loops themselves propagated towards the front of the intrusion. It is interesting to compare these patterns with the observations of Turner & Chen (1974) in a sugar–salt system. From shadowgraphs, they reported that merging occurred at different rates at different horizontal positions, which made it appear as if there were forward-travelling waves on the interface. Tanny & Tsinober (1988) also found a similar merging structure; initiation near the heated wall, completion at the extremity of the intrusion. The fact that merging originates at the heated wall suggests that merging occurs when the thermal boundary layer on the heated sidewall penetrates the salinity interface and locally destroys the salinity step (Bergman & Ungan 1988).

3.5. *The structure of layers when sidewall heating is removed*

As anticipated, in singly stratified experiments the layers stopped propagating when the sidewall heating was removed. It was expected, however, that for the doubly stratified case the initial thermal stratification (unstably stratified) might power the
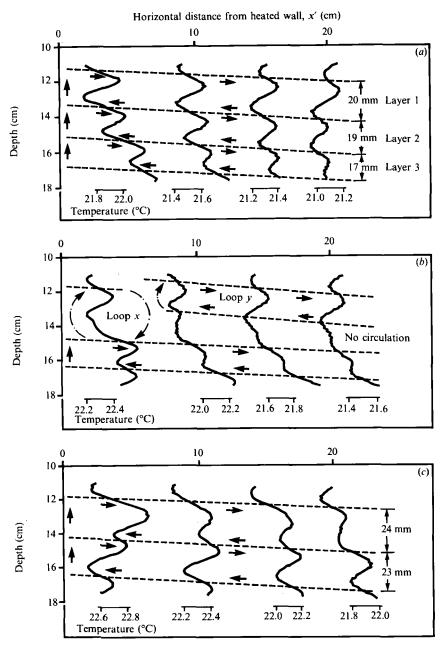
Horizontal distance from heated wall, x' (cm)

FIGURE 14. 'Subsequent' merging pattern of layers for experiment 168. (a) Before merging; $t' = 210$ min, (b) during merging; $t' = 240$ min, (c) after merging; $t' = 315$ min.

layer and keep it propagating when the sidewall heating was removed. But the layers stopped propagating even when the initial density stability ratio, R_ρ, was kept as low as 2.5. This implies that the initial temperature stratification could not energize the intrusions formed by the wall heating.

The temperature profiles taken a few hours after the removal of the wall heating showed the disappearance of the gradient regions as molecular diffusion smeared the profiles. This removal by diffusion is illustrated in figure 15. Using the temperature
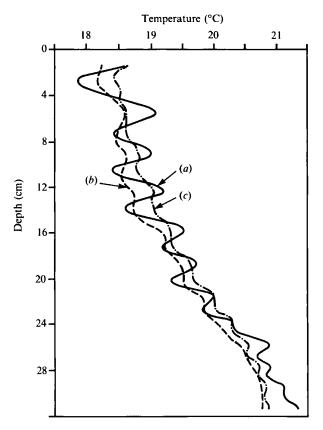
FIGURE 15. Temperature profile for doubly stratified experiment 218. Measured values (a) just prior to the removal of the sidewall heating; (b) 2 h after removal. (c) Computed using the one-dimensional diffusion equation with constant κ_T, taking data given in (a) as initial condition.

profile taken just prior to the removal of the sidewall heating as the initial condition, the one-dimensional diffusion equation

$$\frac{\partial T}{\partial t'} = \kappa_T \frac{\partial^2 T}{\partial z'^2} \tag{29}$$

was solved with insulated top and bottom boundary conditions by finite-difference (implicit) method with constant thermal diffusivity (κ_T) and compared with the actual measurements. Except for an overall loss of heat, the correspondence in shape between the measured and the computed profiles in figure 15 is excellent.

Thus, it is seen from these observations that even with an initial temperature stratification (doubly stratified case), the layers stopped propagating in the absence of the sidewall heating and the vertical temperature profile was relaxed only by molecular diffusion.

4. Conclusion

In both singly and doubly stratified cases it was found that the formation and growth of layers by sidewall heating were generated by a similar mechanism. The layering started when the horizontal Rayleigh number due to sidewall heating

reached a critical value and the lengthscale proposed by Chen *et al.* (1971) was found to adequately express the layer thickness at onset.

For Rayleigh numbers smaller than 10^6, the assumption of locally parallel flow in the core region was found to be reasonable. A model proposed here for the propagation speed of the diffusive intrusion compared well with experimental observation. The validity of the model is constrained by the major assumptions of low aspect ratio and small horizontal Rayleigh numbers. The velocity of propagation was found to increase with decreasing initial density gradient, and also to increase with increasing heat flux through the sidewall.

It was found that the subsequent merging of layers started close to the heated wall, mixing adjacent layers and growing outwards away from the wall. It was noted that the final thickness of the merged layers was not equal to the sum of the later thickness prior to merging; neighbouring layers expanded to a new size, commensurate with the wall temperature at the time.

The hypothesis of internal temperature stratification supplying the heat to keep the circulation in the absence of sidewall heating was found to be not true, at least for the conditions achieved in these experiments. It was found that the convective motion within layers was always triggered and powered by wall heating.

Appendix

Suzukawa & Narusawa (1982) used a constant heat flux of q (W m^{-2}) in their experiments, and in their data analysis assumed the layer thickness to be constant from the wall to the front. However, in reality the layers had a tapered shape and hence were similar to the layers discussed above. Here we discuss their results using the theory of convection in a long shallow cavity.

The constant heat flux imposed at the vertical wall, at $x' = 0$, may be used to define a unit layer heat flux q given by

$$F = H_0 q. \tag{A 1}$$

Inserting (A 1) into (17) and evaluated this at $x' = 0$ leads to

$$\frac{q}{H_0^8} = \frac{\rho c_p g^2 \alpha^2 C_1 K^3}{\kappa_T \nu^2}. \tag{A 2}$$

Now combining (A 2) and (19) and carrying out the double integration with respect to x' leads to a relationship equivalent to (25):

$$\frac{dL'}{dt'} = \frac{9}{4} \frac{q}{(T_w - T_\infty)\rho c_p} = U, \tag{A 3}$$

implying a constant propagation speed. Rearranging leads to

$$\left(\frac{d\bar{T}}{dx}\right) \Big/ \left(-\frac{9}{4} \frac{q}{\rho c_p U^2}\right) = \frac{1}{t}, \tag{A 4}$$
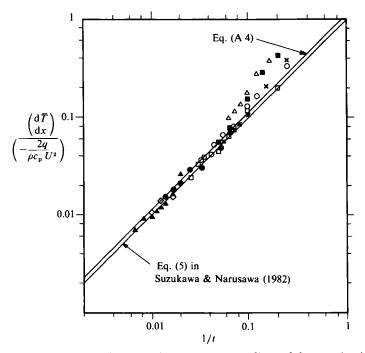
FIGURE 16. Variation of the horizontal temperature gradient of the growing intrusion layer in the constant-heat flux experiments of Suzukawa & Narusawa (1982). The symbols denote their data.

equivalent to (5) in Suzukawa & Narusawa (1982) except for the coefficient $\frac{9}{4}$ which is 2 in their solution. This is the result of allowing h to vary with x'.

Their figure 11 is reproduced in figure 16, including both the solutions. The advantage of the above solution technique is that it clearly displays the role of the convective motion internal to the intruding layers.

REFERENCES

AKBARZADEH, A. & MANNINS, P. 1988 Convective layers generated by side walls in solar ponds. *Solar Energy* **41**, 521–529.

BERGMAN, T. T. & UNGAN, A. 1988 A note on lateral heating in a double-diffusive system. *J. Fluid Mech.* **194**, 175–186.

CARTER, G. D. & IMBERGER, J. 1986 Vertically rising micro-structure profiler. *J. Atmos. Oceanic Technol.* **3**, 462–471.

CHEN, C. F., BRIGGS, D. G. & WIRTZ, R. A. 1971 Stability of thermal convection in a salinity gradient due to lateral heating. *Intl J. Heat Mass Transfer* **14**, 57–65.

CORMACK, D. E., LEAL, L. G. & IMBERGER, J. 1974 Natural convection in a shallow cavity with differentially heated end walls. Part 1. Asymptotic theory. *J. Fluid Mech.* **65**, 209–229.

HEAD, M. J. 1983 The use of miniature four-electrode conductivity probes for high resolution measurement of turbulent density or temperature variations in salt-stratified water flows. Ph.D. thesis, University of California, San Diego.

HUPPERT, H. E., KERR, R. C. & HALLWORTH, M. A. 1984 Heating or cooling a stable compositional gradient from the side. *Intl J. Heat Mass Transfer* **27**, 1395–1401.

HUPPERT, H. E. & TURNER, J. S. 1980 Ice blocks melting into a salinity gradient. *J. Fluid Mech.* **100**, 367–384.

IMBERGER, J. 1974 Natural convection in a shallow cavity with differentially heated end walls. Part 3. Experimental results. *J. Fluid Mech.* **65**, 247–260.

LINDEN, P. F. & WEBER, J. E. 1977 The formation of layers in a double-diffusive system with the sloping boundary. *J. Fluid Mech.* **81**, 757–773.

MILLERO, F. J. & POISSON, A. 1981 Summary of data treatment for the UNESCO one atmosphere equation of state for seawater. *Deep-Sea Res.* **28A**, 625–629.

NARUSAWA, U. & SUZUKAWA, Y. 1981 Experimental study of double-diffusive cellular convection due to a uniform lateral heat flux. *J. Fluid Mech.* **113**, 387–405.

PALIWAL, R. C. & CHEN, C. F. 1980 Double-diffusive instability in an inclined fluid layer. Part 1. Experimental investigation. *J. Fluid Mech.* **98**, 755–768.

PATTERSON, J. & IMBERGER, J. 1980 Unsteady natural convection in a rectangular cavity. *J. Fluid Mech.* **100**, 65–86.

SCHLADOW, S. G. 1985 The dynamics of salt gradient solar pond. Ph.D. thesis, Centre for Water Research, University of Western Australia, Nedlands, Australia.

SCHLADOW, S. G. 1988 Simulation of dynamics of double-diffusive system. *J. Hydraul. Engng Div. ASCE* **114**, 1–20.

SCHLADOW, S. G. & IMBERGER, J. 1987 Sidewall effects in a double diffusive system. *J. Geophys. Res.* **92**(C6), 6501–6514.

SHERMAN, B. G. & IMBERGER, J. 1990 Control of a solar pond. *Solar Energy* (in press).

SUZUKAWA, Y. & NARUSAWA, U. 1982 Structure of growing double diffusive convection cells. *Trans. ASME* C: *J. Heat Transfer* **104**, 248–254.

TANNY, J. & TSINOBER, A. B. 1988 The dynamics and structure of double-diffusive layers in sidewall heating experiments. *J. Fluid Mech.* **196**, 135–156.

THORPE, S. A., HUTT, P. K. & SOULSBY, R. 1969 The effect of horizontal gradients on thermohaline convection. *J. Fluid Mech.* **38**, 375–400.

TURNER, J. S. 1985 Multicomponent convection. *Ann. Rev. Fluid Mech.* **17**, 11–44.

TURNER, J. S. & CHEN, C. F. 1974 Two dimensional effects in double diffusive convection. *J. Fluid Mech.* **63**, 577–592.

WIRTZ, R. A. & REDDY, C. S. 1979 Experiments on convective layer formation and merging in a differentially heated slot. *J. Fluid Mech.* **91**, 451–464.